

Tree Tensor Networks Methods for Efficient Calculation of Molecular Vibrational Spectra

Shuo Sun ,^{a)} Richard M. Milbradt ,¹ Stefan Knecht ,² Chandan Kumar ,³ and Christian B. Mendl ,^{1, 4, b)}

¹⁾ *Technical University of Munich, CIT, Department of Computer Science,
Boltzmannstraße 3, 85748 Garching, Germany*

²⁾ *Algorithmiq Ltd, Kanavakatu 3C, FI-00160 Helsinki, Finland*

³⁾ *BMW Group, Munich*

⁴⁾ *Technical University of Munich, Institute for Advanced Study,
Lichtenbergstraße 2a, 85748 Garching, Germany*

(Dated: 19 December 2025)

We develop and employ general Tree Tensor Networks (TTNs) to compute the vibrational spectra for two model systems: a set of 64-dimensional coupled oscillators and acetonitrile. We explore various tree architectures, ranging from the simple linear structure of Matrix Product States (MPS), to trees where only the leaf nodes carry a physical leg—as seen in the underlying ansatz of the Multilayer Multiconfiguration Time-Dependent Hartree (ML-MCTDH) method—and further to more general trees in which all nodes are allowed to possess a physical leg. In addition, we implement Locally Optimal Block Preconditioned Conjugate Gradient (LOBPCG) methods and Inverse Iteration methods as eigensolvers. By means of comprehensive benchmarking of runtime and accuracy, we demonstrate that sub-wavenumber accuracy in vibrational spectra is achievable with all TTN structures. MPS and three-legged tree tensor network states (T3NS) have similar runtimes, whereas leaf-only trees require significantly more time. All numerical simulations were performed using PyTreeNet, a Python package designed for flexible tensor network computations.

^{a)} Electronic mail: shuo.sun@tum.de

^{b)} Electronic mail: christian.mendl@tum.de

I. INTRODUCTION

Vibrational spectroscopies, such as IR and Raman spectroscopies, are widely used in chemistry to characterize molecules. However, interpreting such spectra is not always straightforward, as the vibrational degrees of freedom scale as $3N - 6$ (where N is the number of nuclei), making numerical simulations crucial for structure and property determination. In recent years, numerous methods have been developed to obtain vibrational spectra, such as VSCF^{1–4}, VCI^{5–8}, VCCSD^{9–12}, neural network methods¹³, and quantum simulation^{14,15}. VSCF is a mean-field theory and often lacks the accuracy required for the desired applications. Although VCI, VCCSD, and neural networks can provide accurate calculations, they do so at a high computational cost. Quantum simulation methods also incur high costs when simulated classically or require quantum hardware beyond current near-term device capabilities.

As a promising addition to the available methods, tensor network methods have made significant progress in vibrational spectra calculations in recent years^{16–23}. However, most implementations have used matrix product operators (MPOs) to represent the Hamiltonian. This approach limits the full potential of tensor network methods, as the molecules' normal modes exhibit long-range interactions, while the MPO formalism primarily favors nearest-neighbor interactions. This structural limitation is particularly problematic when focusing on higher-lying excited eigenstates, where energy degeneracy becomes significant, making accurate eigenstate computation even more challenging. To this end, we propose in this paper an approach that utilizes tree tensor network operators (TTNOs)^{24,25} to represent the Hamiltonian and likewise tree tensor network states (TTNSs)^{26,27} to represent the state function for eigenvalue problem calculations, thereby fully leveraging tree structure connectivity. We implement the LOBPCG method and inverse iteration method within the tree tensor network framework to solve the eigenvalue problem. We demonstrate sub-wavenumber accuracy on two benchmark systems — 64-dimensional coupled oscillators and acetonitrile^{28,29} — and compare runtime and accuracy across different tree structures (MPS, T3NS²⁷, and leaf-only trees). All computations were performed with PyTreeNet³⁰.

II. METHODS

In this section, we first briefly introduce tree tensor networks in Sec. (II A). We then discuss two well-known numerical eigenvalue algorithms in Sec. (II B). Finally, we combine these two aspects and introduce our implementation of these numerical algorithms within the tensor network framework in Sec. (II C).

A. Tree Tensor Network Operations

1. *Introduction to Tensor Networks*

The field of tensor networks has seen significant research activity over the last two decades. It has been especially successful when applied to the numerical simulation of quantum systems. We will restrict this introduction to the concepts relevant to the present work. For a deeper and pedagogical introduction, refer to^{31–34}, and for a general overview, see the recent reviews^{35–37}. In general, a tensor is an element $A \in \mathbb{C}^{\times_{i=1}^N D_i}$, i.e., a multi-dimensional array whose entries are identified by a string of N indices, where the i th index can take values in $\{1, \dots, D_i\}$. Intuitively, this is a generalization of vectors and matrices, where the entries are identified by one and two indices, respectively. We will call N the *degree* of a tensor, while we refer to the different indices on a tensor as *legs*.

If a leg i of a tensor A and a leg i' of a different tensor B have the same dimension $D_i = D_{i'}$, we can contract over these legs by summing over the products of the tensor entries with the same index for the contracted legs. Let us emphasize this with an example, where $A \in \mathbb{C}^{D_1 \times D_2 \times D_3}$ and $B \in \mathbb{C}^{D_2 \times D_4 \times D_5}$. Here we can contract the second leg of A with the first leg of B , leading to a new tensor $C \in \mathbb{C}^{D_1 \times D_3 \times D_4 \times D_5}$. The entries of C are defined by

$$C_{jklm} = \sum_{n=1}^{D_2} A_{jnk} B_{nlm}. \quad (1)$$

Now, a *tensor network* is simply a collection of tensors and a record of the legs that are contracted. To facilitate easier readability, a graphical notation for tensor networks is available. One can build this representation by depicting every tensor as a geometrical shape and attaching one line per leg. Then, all lines representing contracted legs are connected to

their corresponding partners. For example, Eq. (1) can be depicted as

$$\begin{array}{c} j \\ | \\ \text{C} \\ | \\ k \end{array} \ell = \begin{array}{c} j \\ | \\ \text{A} \\ | \\ k \end{array} n \begin{array}{c} j \\ | \\ \text{B} \\ | \\ m \end{array} \ell. \quad (2)$$

We can also split a tensor. To this end, we can reinterpret a tensor as a matrix by defining which legs should be the output and input legs of the matrix. Then we can apply any desired matrix decomposition, the most common being the QR decomposition and the singular value decomposition (SVD). For example, we can obtain two tensors, say A' and B' , from a tensor C by first reshaping C into a matrix. This is done by grouping some of its legs to form the ‘row’ indices and the remaining legs to form the ‘column’ indices. After applying a matrix decomposition (e.g., SVD or QR), the resulting matrices can be reshaped back into tensors, effectively splitting the original tensor C into two or more tensors. These two kinds of tensor manipulation allow us to represent an arbitrary quantum state as a tensor network, as we discuss in the next section.

2. Tensor Network States and Operators

A quantum state $|\psi\rangle$ generally has a large number of degrees of freedom scaling exponentially in system size. For example, if we have a quantum system consisting of L smaller quantum systems, we can write the state as

$$|\psi\rangle = \sum_{s_1, \dots, s_L} C_{s_1, \dots, s_L} |s_1, \dots, s_L\rangle, \quad (3)$$

where $\{|s_j\rangle\}$ is the basis of the local quantum system j . Repeated tensor decompositions allow us to express the tensor C as a tensor network with an arbitrary underlying tree shape

$$|\psi\rangle = \sum_{\substack{s_1, \dots, s_L \\ v_1, \dots, v_M}} T_{\{v_1, i\}, s_1}^{(1)} \dots T_{\{v_L, i\}, s_L}^{(L)} |s_1, s_2, \dots, s_L\rangle, \quad (4)$$

where we assumed for simplicity of notation that every tensor has one uncontracted leg s_j . Here s_j indexes the *physical* (local system) degrees of freedom with dimension called the physical leg dimension, while $v_{(j,i)}$ indexes the *virtual* (internal) degrees of freedom connecting tensors in the network. The dimension of v_i is denoted as virtual bond dimension. The total number of contracted legs in the tensor network is M and $\{v_{j,i}\} \subset \{v_1, \dots, v_M\}$

are the contracted legs of tensor $T^{(j)}$. The tensor network in Eq. (4) is a *tree tensor network state (TTNS)* if there are no loops in the network²⁶.

We can apply the analogous decomposition to a quantum operator acting on high-dimensional systems, yielding

$$\hat{O} = \sum_{\substack{p_1, \dots, p_L \\ q_1, \dots, q_L \\ v_1, \dots, v_M}} \mathcal{T}_{\{v_1, i\}, p_1, q_1}^{(1)} \cdots \mathcal{T}_{\{v_L, i\}, p_L, q_L}^{(L)} |p_1, p_2, \dots, p_L\rangle \langle q_1, q_2, \dots, q_L|. \quad (5)$$

This tensor network is called a *tree tensor network operator (TTNO)*²⁴ and differs from a TTNS mostly in that every site has two uncontracted physical legs rather than just one. A graphical depiction of an example TTNS and TTNO based on the same tree is shown in Figure 1.

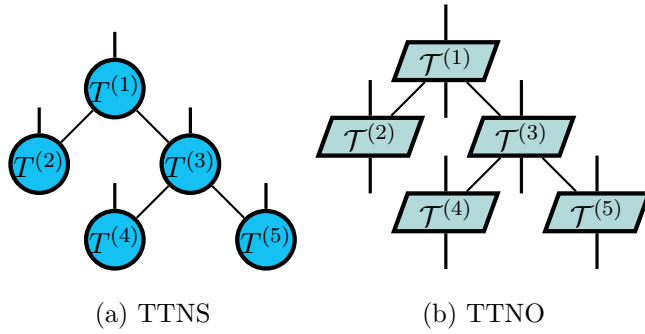


FIG. 1. Examples of a TTNS and TTNO with the same tree topology, differing in the number of physical legs per tensor. Adapted from³⁸.

3. TTNO construction

To construct a TTNO representing a desired system Hamiltonian, we use the algorithm introduced in Ref. 38, which improves upon the methods introduced in Refs. 25 and 39. The algorithm starts from a Hamiltonian in the form

$$H = \sum_{i=1}^N c_i \bigotimes_{j=1}^L A_i^{(j)}, \quad (6)$$

where $A_i^{(j)}$ is an operator acting on the j -th subsystem (or site). We denote the overall number of subsystems by L . Once we have decided on a desired tree structure, we rewrite the Hamiltonian as a state diagram²⁵. This is a symbolic representation method for arbitrary

tree tensor network topologies. Initially, the state diagrams of each of the N terms are unconnected. Note that cutting any edge in a tree will cut the tree into two parts. Doing this will also cut the state diagram into two separate sets of unconnected hypergraphs. These two sets can be seen as the two parts of a binary graph, where the connecting edges are the original connections in the state diagram. We combine equal-valued elements on each side of the graph and minimize the connectivity between the two sets via the algorithm described in Ref. 38. The algorithm uses symbolic Gaussian elimination and the vertex cover method to reduce the connectivity, while keeping prefactors of every term in consideration. Notably, minimizing the connectivity of a bipartite graph over an edge is equivalent to minimizing the bond dimension in the final TTNO. We perform this connectivity minimization for every edge in the tree structure. As a final step, we translate the compressed state diagram to a TTNO as described in Ref. 25.

B. Numerical Algorithms

The eigensolvers we employ—LOBPCG and Inverse Iteration—require several TTN-specific operations detailed in Sec. (II C): computing $H|x\rangle$ via zip-up (Sec. (II C 1)), compressing sums of states via variational fitting (Sec. (II C 2)), and solving linear systems $H|y\rangle = |x\rangle$ via alternating least squares (ALS, Sec. (II C 3)). In the following, we first outline the generic algorithms, and then describe their implementation specialized to TTNs.

1. *Locally Optimal Block Preconditioned Conjugate Gradient (LOBPCG) method*

Locally Optimal Block Preconditioned Conjugate Gradient (LOBPCG) is a numerical method to solve eigenvalue problems^{40,41}. It is a generalization of the conjugate gradient method, which is very efficient for large sparse matrices. In this work, we adapt LOBPCG to tree tensor networks. The core idea is to construct, at each iteration, a search subspace spanned by the current approximate eigenvector, its residual, and the previous search direction, and then solve a Rayleigh–Ritz problem within this subspace.

We begin by initializing the residual vector as $r = Hx - \lambda x$, where x is the current state

vector and λ is the Rayleigh quotient,

$$\lambda = \frac{x^\dagger H x}{x^\dagger x}. \quad (7)$$

In this work we use the three-term recurrence formulation of LOBPCG,

$$p^{(k)} = \beta r^{(k)} + \gamma p^{(k-1)} \quad (8a)$$

$$\tilde{x}^{(k+1)} = \alpha x^{(k)} + p^{(k)} \quad (8b)$$

$$x^{(k+1)} = \frac{\tilde{x}^{(k+1)}}{\|\tilde{x}^{(k+1)}\|} \quad (8c)$$

where the coefficients α , β , and γ are obtained by solving the small generalized eigenvalue problem

$$\begin{bmatrix} x^{(k)} \\ r^{(k)} \\ p^{(k)} \end{bmatrix} H \begin{pmatrix} x^{(k)} & r^{(k)} & p^{(k)} \end{pmatrix} \begin{pmatrix} \alpha \\ \beta \\ \gamma \end{pmatrix} = \lambda \begin{bmatrix} x^{(k)} \\ r^{(k)} \\ p^{(k)} \end{bmatrix} \begin{pmatrix} x^{(k)} & r^{(k)} & p^{(k)} \end{pmatrix} \begin{pmatrix} \alpha \\ \beta \\ \gamma \end{pmatrix}. \quad (9)$$

This method can also be implemented in a block manner, where we compute N eigenvalues and eigenvectors simultaneously by constructing $x^{(k)}$, $r^{(k)}$, and $p^{(k)}$ for each eigenvector and solving a $3N \times 3N$ generalized eigenvalue problem. This block formulation is particularly important for handling near-degenerate states (as mentioned in [Sec. \(I\)](#)), as it solves for multiple eigenstates within the same subspace, preventing convergence to the same state.

To accelerate convergence, we can apply a preconditioner M to the residual vector, which is typically an approximation of the inverse of the shifted Hamiltonian,

$$r_{\text{precond}} = Mr = (H - s\mathcal{I})^{-1}r, \quad (10)$$

where s is the shift value and \mathcal{I} is the identity matrix. The preconditioned residual can be obtained by solving the linear system

$$(H - s\mathcal{I})r_{\text{precond}} = r. \quad (11)$$

In the tree tensor network framework, we solve this equation by iterating through the network nodes (called sweeps), optimizing one tensor at a time, as described in [Sec. \(II C 3\)](#).

The pseudocode of the single and block LOBPCG method is shown in [Algorithm 1](#) and [Algorithm 2](#), respectively. Note that at the start of the first iteration, the search directions

are initialized as $p^{(0)} = r^{(0)}$. For all subsequent iterations, $p^{(i)}$ is updated from the generalized eigenvector components according to [Eq. \(8\)](#).

Algorithm1 LOBPCG for a Single State

Input: Matrix H , initial state vector $x^{(0)}$, shift for preconditioner s , max iterations N_{iter}

Output: Converged state x and eigenvalue λ

```

1: Initialize:  $x \leftarrow x^{(0)}$ ,  $\lambda \leftarrow \frac{x^\dagger H x}{x^\dagger x}$ 
2: for  $i = 1$  to  $N_{\text{iter}}$  do
3:   Compute residual:  $r \leftarrow Hx - \lambda x$   $\triangleright$  Zip-up (Sec. \(II C 1\)), variational fitting (Sec. \(II C 2\))
4:   Apply preconditioner:  $r \leftarrow Mr$   $\triangleright$  See Eq. \(10\), via alternating least squares (ALS)
5:   Build subspace:  $\mathcal{S} \leftarrow \{x, r, p\}$   $\triangleright$  For  $i = 1$ , set  $p \leftarrow r$ 
6:   if orthogonalization required then
7:     Orthogonalize all vectors in  $\mathcal{S}$  against the constraint subspace  $\triangleright$  e.g., previously
       computed lower-lying eigenstates
8:   end if
9:   Construct matrices:  $\tilde{H}_{kl} \leftarrow s_k^\dagger H s_l$ ,  $\tilde{M}_{kl} \leftarrow s_k^\dagger s_l$  for  $s_k, s_l \in \mathcal{S}$ 
10:  Solve generalized eigenvalue problem:  $\tilde{H}\mathbf{v} = \lambda \tilde{M}\mathbf{v}$ ,  $\mathbf{v} = (\alpha, \beta, \gamma)^T$ 
11:  Update  $x, p$  from eigenvectors,  $\lambda \leftarrow$  smallest eigenvalue  $\triangleright$  See Eq. \(8\)
12: end for
13: return  $x, \lambda$ 

```

2. Inverse Iteration method

Inverse iteration is an iterative method to find the eigenvector and eigenvalue of a matrix close to a given shift value. The basic idea is that

$$\tilde{x}^{(i+1)} = (H - s\mathcal{I})^{-1}x^{(i)} \quad (12a)$$

$$x^{(i+1)} = \frac{\tilde{x}^{(i+1)}}{\|\tilde{x}^{(i+1)}\|} \quad (12b)$$

where again s is the shift value and \mathcal{I} the identity matrix. When s is not exactly one of the eigenvalues of H , we can obtain the updated eigenvector by solving the linear system $(H - s\mathcal{I})x^{(i+1)} = x^{(i)}$ by sweeping through the tensor network, similar to [Eq. \(11\)](#). In this work, we found the solution of the linear system using the alternating least squares (ALS)

Algorithm2 Block LOBPCG for Multiple States

Input: Matrix H , initial state vector $\{x_j^{(0)}\}_{j=1}^n$, shift for preconditioner s , max iterations N_{iter}

Output: Multiple eigenstates $\{x_j\}_{j=1}^n$ and eigenvalues $\{\lambda_j\}_{j=1}^n$

```

1: Initialize:  $\{x_j\}_{j=1}^n \leftarrow \{x_j^{(0)}\}_{j=1}^n$ ,  $\{\lambda_j\}_{j=1}^n \leftarrow \left\{ \frac{x_j^\dagger H x_j}{x_j^\dagger x_j} \right\}_{j=1}^n$ 
2: for  $i = 1$  to  $N_{\text{iter}}$  do
3:   for  $j = 1$  to  $n$  do
4:     Compute residual:  $r_j \leftarrow Hx_j - \lambda_j x_j$  ▷ Zip-up, variational fitting
5:     Apply preconditioner:  $r_j \leftarrow Mr_j$  ▷ See Eq. (10), via alternating least squares (ALS)
6:     if orthogonalization required then
7:       Orthogonalize  $x_j$ ,  $r_j$  and  $p_j$  against the constraint subspace
8:     end if
9:   end for
10:  Build subspace:  $\mathcal{S} \leftarrow \{x_j\}_{j=1}^n \cup \{r_j\}_{j=1}^n \cup \{p_j\}_{j=1}^n$ 
11:  Construct matrices:  $\tilde{H}_{k\ell} \leftarrow s_k^\dagger H s_\ell$ ,  $\tilde{M}_{k\ell} \leftarrow s_k^\dagger s_\ell$  for  $s_k, s_\ell \in \mathcal{S}$ 
12:  Solve generalized eigenvalue problem:  $\tilde{H}\mathbf{v} = \lambda \tilde{M}\mathbf{v}$ 
13:  for  $j = 1$  to  $n$  do
14:    Update state:  $x_j \leftarrow \sum_{k=1}^n v_{k,j} s_k$ 
15:     $p_j \leftarrow \sum_{k=n+1}^{3n} v_{k,j} s_k$  ▷ See Eq. (8)
16:  end for
17:  Update eigenvalues:  $\{\lambda_j\}_{j=1}^n \leftarrow$  smallest  $n$  eigenvalues
18: end for
19: return  $\{x_j\}_{j=1}^n$ ,  $\{\lambda_j\}_{j=1}^n$ 

```

method, which is described in Sec. (II C 3). The shift value can stay the same throughout the iterations and may also be updated after one or few iterations. In this project, we cluster eigenvalues into groups and use block inverse iteration to solve the eigenproblem. Clustering is particularly important for near-degenerate eigenvalues where individual shifts might miss multiple closely spaced states. We use the mean Rayleigh quotient of the group as the shift value and update the Rayleigh quotient in each iteration. The pseudocode of the block inverse iteration method is described in Algorithm 3.

Algorithm3 Block Inverse Iteration

Input: Matrix H , initial state vector $\{x_j^{(0)}\}_{j=1}^n$, max iterations N_{iter} , multiple eigenstates $\{x_j\}_{j=1}^n$ and eigenvalues $\{\lambda_j\}_{j=1}^n$

1: Initialize: $\{x_j\}_{j=1}^n \leftarrow \{x_j^{(0)}\}_{j=1}^n$, $\{\lambda_j\}_{j=1}^n \leftarrow \left\{ \frac{x_j^\dagger H x_j}{x_j^\dagger x_j} \right\}_{j=1}^n$

2: **for** $i = 1$ to N_{iter} **do**

3: Update shift and Hamiltonian: $s \leftarrow \frac{1}{n} \sum_{j=1}^n \lambda_j$, $H_{\text{shift}} \leftarrow H - s\mathcal{I}$

4: **for** $j = 1$ to n **do**

5: Solve $H_{\text{shift}} y_j = x_j$, update state: $x_j \leftarrow y_j / \|y_j\|$ ▷ Solve with ALS [Sec. \(II C 3\)](#)

6: **end for**

7: **if** $n > 1$ **then**

8: Orthogonalize vectors by solving generalized eigenvalue problem

9: $\tilde{H}_{k\ell} \leftarrow x_k^\dagger H x_\ell$, $\tilde{M}_{k\ell} = x_k^\dagger x_\ell$, $\tilde{H}\mathbf{v} = \lambda \tilde{M}\mathbf{v}$, $x_j \leftarrow \sum_k v_{jk} x_k$

10: **end if**

11: **end for**

12: **return** $\{x_j\}_{j=1}^n$, $\{\lambda_j\}_{j=1}^n$

C. Implementation of LOBPCG and Inverse Iteration on Tree Tensor Networks

1. Zip-Up method

The zip-up method is a technique to compute the product of a tree tensor network operator H and a tree tensor network state x . It was initially developed for linear structures⁴², though we extend it here to arbitrary tree structures. The naive approach to applying a TTNO to a TTNS is to perform the contraction for every pair of state and operator tensors, followed by a compression sweep using SVD. However, this method scales rather badly with the bond dimension of the TTNS and TTNO (see [Appendix A](#)). Therefore, we utilize the zip-up method, which circumvents the worst scaling parts of the naive contraction. The zip-up method starts at the TTNs' leaf nodes. For each leaf ℓ , the algorithm contracts the TTNO leaf tensor $\mathcal{T}^{(\ell)}$ with the corresponding TTNS leaf tensor $T^{(\ell)}$, and then factorizes the resulting tensor into two separate tensors. In this work, we use a rank-revealing QR decomposition, yielding $A = QR$; subsequently, we truncate the Q matrix to reduce the

cost. The resulting Q matrix becomes the new tensor for the TTNS node, while the R matrix is absorbed into the next site's tensor for the TTNO-TTNS product. This procedure is repeated for all but one node of the TTNO and TTNS are fully contracted. For TTNs, we must process child nodes before parents to respect the tree hierarchy, starting from leaf nodes and proceeding towards parent nodes. For the final, i.e. root node, we only perform the contraction. Overall one can encounter a high computational cost when contracting nodes with three virtual legs. However, the physical legs for those nodes typically have a bond dimension of 1. Therefore, we can use a smarter contraction scheduling to decide whether to contract the virtual legs of the TTNO or TTNS to the R matrix first. This optimization reduces the cost for T3NS to be similar to MPS contraction. The zip-up procedure is depicted in Figure 2.

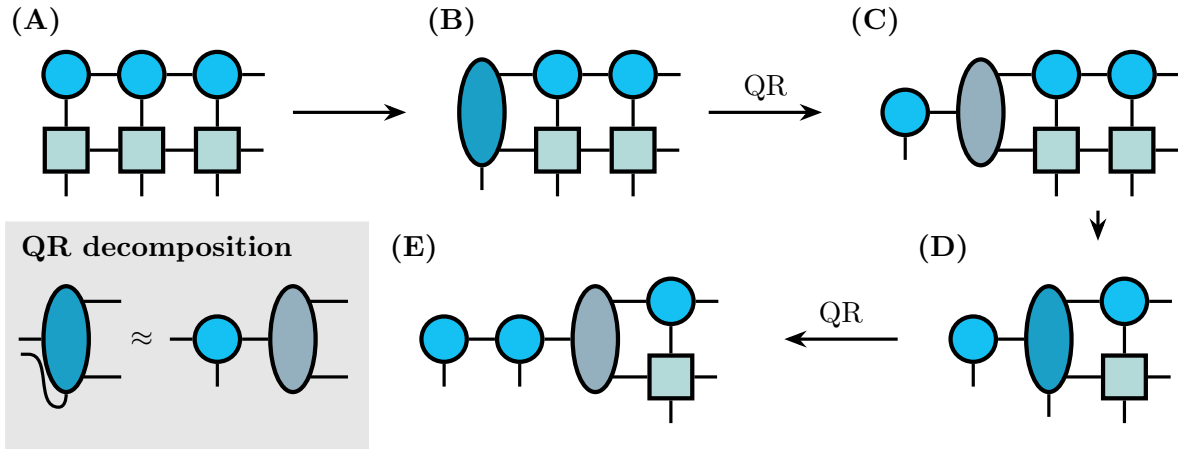


FIG. 2. Illustration of the zip-up method. Circle tensors represent the state, square tensors represent the operator, and ellipses are intermediate tensors, for example, the R tensor. When contracting a local site tensor of the state and a local site tensor of the operator into an intermediate ellipse tensor, as shown in steps (C) to (D), one can optimize the contraction order to minimize the computational cost.

2. Variational Fitting

Variational fitting is a method that can be used to compress the sum of multiple TTNSs, or multiple TTNOs applied to TTNSs, into a single TTNS ψ , i.e.,

$$\psi \approx \sum_i c_i O_i \phi_i, \quad (13)$$

where the O_i are TTNOs, ϕ_i are TTNSs, and c_i are complex coefficients. When the O_i are identity operators, the aforementioned equation is equivalent to compressing the sum of multiple weighted TTNSs. The idea behind this compression is to find the best fit by minimizing the difference between the compressed and uncompressed TTNSs:

$$\min_{\psi} \left\| \psi - \sum_i c_i O_i \phi_i \right\|_2 \quad (14)$$

by iteratively updating the ψ tensors. At each node j , we construct an effective Hamiltonian $H_{\text{eff},j}$ by contracting our current estimate of the TTNS ψ with its complex conjugate ψ^* except for the tensor ψ_j at node j and its complex conjugate counterpart. Then we need to solve the linear system

$$H_{\text{eff},j} y_j = \sum_i c_i O_{\text{eff},i,j} \phi_{i,j}, \quad (15)$$

where y_j is the solution tensor at the current site, $O_{i,j}$ is the local TTNO tensor at the current site, and $\phi_{i,j}$ is the local TTNS tensor at the current site. A graphical version of this equation for MPS is depicted in [Figure 3](#). The above linear system of equations is solved using the Minres algorithm from Scipy⁴³. The obtained solution tensor y_j then updates the current ψ_j tensor. Since we perform one-site updates at a time, the virtual bond dimension of the solution tensor network state will not change. To enable dynamic bond dimension updates, we further compute the local residuals after solving the linear system

$$r = H_{\text{eff},j} y_j - \sum_i c_i O_{i,j} \phi_{i,j}. \quad (16)$$

If the norm of this residual vector is larger than a given threshold, we apply a rank-revealing QR decomposition and expand the solution y_j with the obtained Q .

The ability to compress sums of TTNSs makes variational fitting useful inside the LOBPCG method. We will next consider the alternating least squares approach and its adaptation to TTNs within the LOBPCG eigenvalue solver.

3. *Alternating least squares (ALS) method*

To solve the linear system $H\psi = \phi$ in a tree tensor network framework, i.e., where H is represented as a TTNO and ψ and ϕ are TTNS, we implement the alternating least squares (ALS) method. ALS is an iterative method to solve local linear system equations. Similar

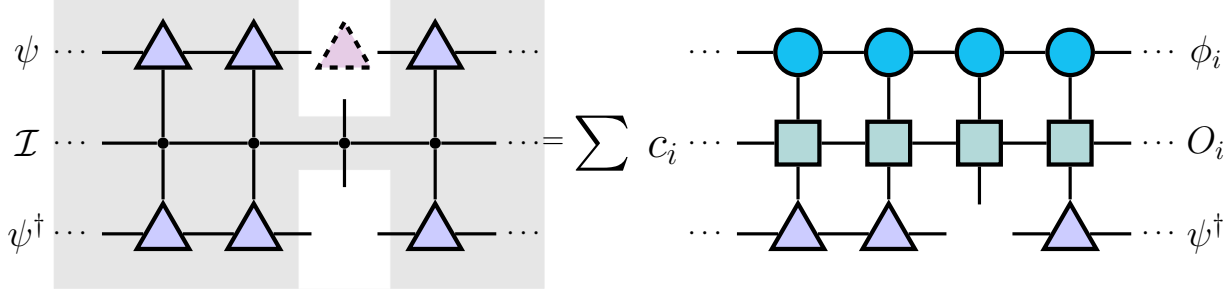


FIG. 3. Variational fitting. Circle tensors are the given state ϕ_i , square tensors are the given operator O_i , and triangle tensors are the target state ψ . The tensors in the shaded area on the left represent the effective Hamiltonian A . The dashed triangle tensor is the solution of the linear system $Ax = b$. The right-hand side represents the vector b after contraction.

to variational fitting, we update our solution node by node. For each node, we have a local, smaller system of linear equations to solve. When updating node ϕ_j , we construct the local effective Hamiltonian $H_{\text{eff},j}$ by contracting all other nodes, effectively computing $\langle \psi | H | \psi \rangle$, except for the current node ϕ_j and its conjugate counterpart. The effective right-hand side vector resembles the contraction of $\langle \psi | \phi \rangle$ but leaving out ψ^* . A graphical depiction of the equation to solve is shown in Figure 4. Minres can find the local best fit for the current node, denoted $\tilde{\psi}_j$. We then replace the old node tensor ψ_j with the new solution tensor $\tilde{\psi}_j$ and move to the next node. This iteration over all nodes in the tree constitutes one sweep; multiple sweeps are typically required for convergence. Since this method is only used for approximating the preconditioned residual vector in LOBPCG, we do not need to fully converge the solution. In practice, running two sweeps is typically sufficient to obtain an accurate approximation. For the inverse iteration method, we can increase the accuracy by performing more sweeps. The difference between variational fitting and ALS is in how the local effective Hamiltonian is constructed. In variational fitting, the local effective Hamiltonian is constructed by contracting the bra ψ and the ket ψ tensors with an identity operator, i.e., $\langle \psi | I | \psi \rangle$, whereas in ALS, the local effective Hamiltonian is constructed by contracting $\langle \psi | H | \psi \rangle$.

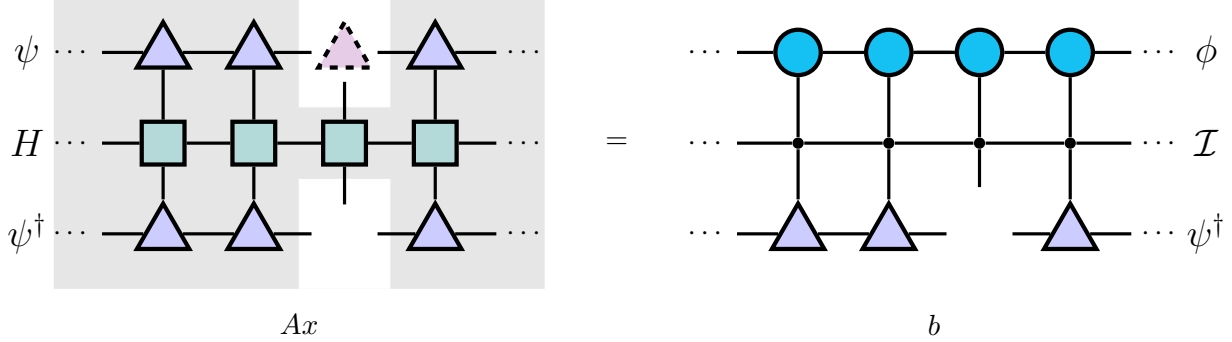


FIG. 4. Alternating least squares. Circle tensors are the given state ϕ , square tensors are the given operator H , and triangle tensors are the target state ψ . The tensors in the shaded area on the left represent the effective Hamiltonian A . The dashed triangle tensor is the solution of the linear system $Ax = b$. The right-hand side represents the vector b after contraction.

III. RESULTS

In the following, we assess the numerical performance and accuracy of our TTN framework for two benchmark systems — 64-dimensional coupled oscillators and acetonitrile^{28,29} — and compare runtime and accuracy across different tree structures (MPS, T3NS²⁷, and leaf-only trees¹⁷). The corresponding tree structures are described in Appendix B. All computational codes and results are publicly available on GitHub (<https://github.com/sunshuo987/vibcal>). Benchmark calculations were carried out on Intel Core i7-10700 processors with 16 cores and 32 GB of RAM; however, the actual simulations required substantially less memory.

A. 64-dimensional coupled oscillators

The vibrational Hamiltonian of bilinearly coupled oscillators is described by

$$H = \sum_{i=1}^D \frac{\omega_i}{2} \left(-\frac{\partial^2}{\partial q_i^2} + q_i^2 \right) + \sum_{j=1}^{D-1} \sum_{i>j}^D \alpha_{ij} q_i q_j. \quad (17)$$

We set $D = 64$, $\omega_j = \sqrt{\frac{j}{2}}$, and $\alpha_{ij} = 0.1$. These parameters create a moderately coupled system that tests the ability of TTN methods to handle bilinear interactions. In this work,

we use Hermite basis functions for which the kinetic term in Eq. (17) is given by^{44,45}

$$T_{mn} = \begin{cases} (-1)^{m-n} \left(\frac{2}{(x_m - x_n)^2} - \frac{1}{2} \right), & m \neq n, \\ \frac{1}{6} (4N - 1 - 2x_m^2), & m = n, \end{cases} \quad (18)$$

and q_m is a diagonal matrix with diagonal entries $= (x_1, x_2, \dots, x_k)$, where x_i are the roots of the Hermite polynomials.

We represent both the state and the Hamiltonian using MPS and T3NS tree structures, as illustrated in Appendix B Figure 7. Each oscillator is assigned a physical basis size of 8, and the maximum virtual bond dimension of the states is set to 5. We compute the lowest 30 eigenstates using the LOBPCG algorithm. For this model, the exact energy levels are available analytically; the corresponding absolute errors are plotted in Figure 5. Both MPS and T3NS achieve errors below 10^{-2} cm⁻¹ for all low-lying states; however, T3NS consistently yields smaller errors than MPS. This result demonstrates the improved accuracy of tree tensor network representations and highlights their potential advantages over one-dimensional MPS for capturing correlations in vibrational Hamiltonians.

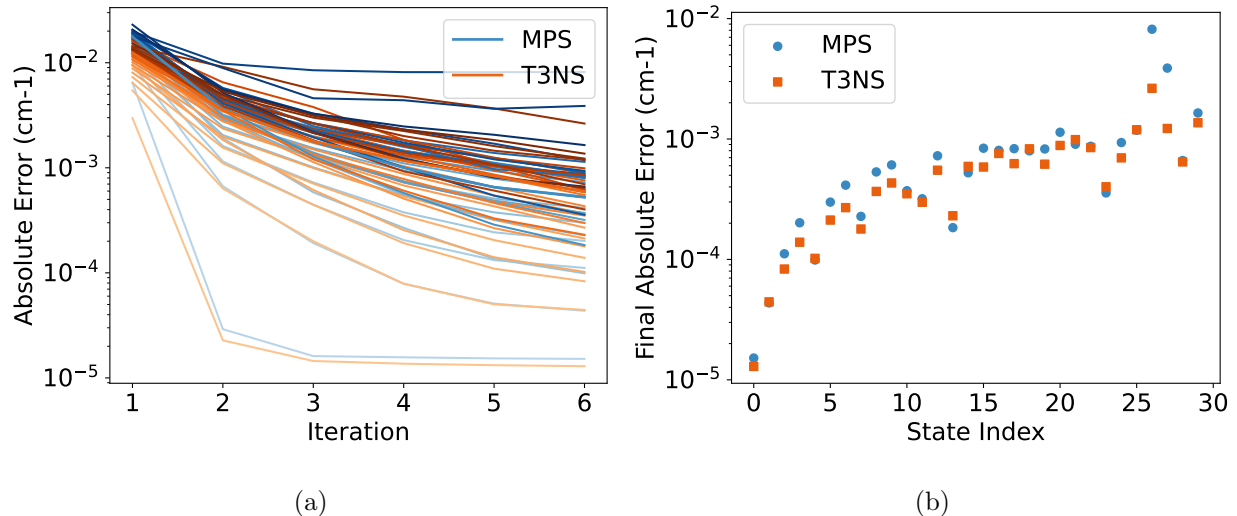


FIG. 5. (a) Convergence curves over six iterations for the lowest 30 eigenstates of the 64-dimensional coupled-oscillator model, computed using the MPS and T3NS ansatz. Color intensity encodes the energy level, with lighter shades corresponding to lower energies. (b) Final absolute error for both structures.

B. Acetonitrile (CH3CN)

Acetonitrile is a molecule with 12 vibrational modes (see Figure 6a) that has been studied extensively in recent years^{16,17,23,28,29,46}. The C_{3v} symmetry of acetonitrile results in degenerate vibrational modes and strong anharmonic coupling between them, which poses significant challenges for standard eigensolvers. In this work, we employed the conventional local basis sizes, which are $\{9, 7, 9, 9, 9, 9, 7, 7, 9, 9, 27, 27\}$, and adopted the same coupling strengths reported in the literature^{13,46}. The vibrational Hamiltonian of acetonitrile used in these references has the form

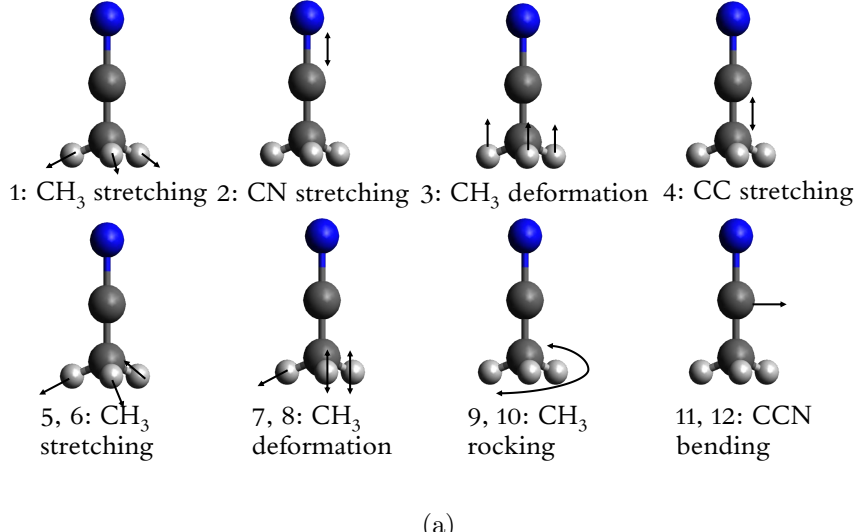
$$H = -\frac{1}{2} \sum_i \omega_i \frac{\partial^2}{\partial q_i^2} + \frac{1}{2} \sum_i \omega_i q_i^2 + \frac{1}{6} \sum_{i,j,k} k_{i,j,k}^{(3)} q_i q_j q_k + \frac{1}{24} \sum_{i,j,k,\ell} k_{i,j,k,\ell}^{(4)} q_i q_j q_k q_\ell, \quad (19)$$

where $k^{(3)}$ and $k^{(4)}$ are the cubic and quartic force constants, and indices i, j, k, ℓ represent the 12 vibrational modes.

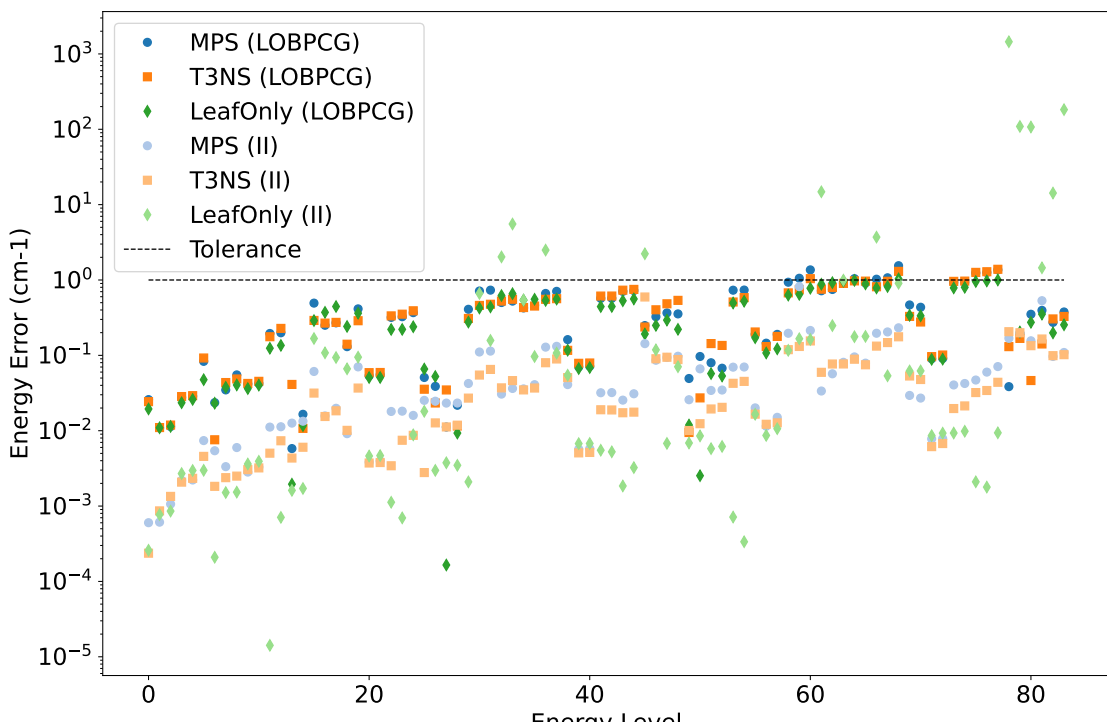
We first applied the LOBPCG method to compute the lowest 84 eigenstates with a maximum virtual bond dimension of 12. These eigenstates were then used as initial guesses for the Inverse Iteration method in order to obtain higher-accuracy solutions. This two-stage strategy balances computational efficiency and precision: LOBPCG provides high-quality starting vectors, which Inverse Iteration subsequently refines. For the Inverse Iteration calculations, the maximum virtual bond dimension was increased to 20. We note that the numerical accuracy could in principle be further improved by enlarging the bond dimensions. All results are summarized in Table II.

In this example, we compare three tensor network structures: MPS, T3NS, and a leaf-only tree, in which only leaf nodes carry physical legs. The tree structures are illustrated in Appendix B Figure 8. Analyzing the LOBPCG results for the lowest 84 eigenvalues, the leaf-only tree with virtual bond dimension 12 yields the smallest absolute error for 57 eigenstates, while MPS and T3NS do so for 12 and 15 eigenstates, respectively. The mean errors of the three structures are comparable (0.385 for MPS, 0.354 for T3NS, and 0.317 for the leaf-only tree). Although the leaf-only tree achieves the highest accuracy in this stage, its runtime is 50% longer than that of MPS and 31% longer than that of T3NS.

When considering the full two-stage workflow (LOBPCG followed by Inverse Iteration), shown in the rightmost columns of Table II, the leaf-only tree encounters convergence diffi-



(a)



(b)

FIG. 6. (a) Motion of the 12 vibrational modes of acetonitrile (CH_3CN). (b) Final absolute error of the 84 eigenstates computed via MPS, T3NS and leaf-only tensor network structures.

culties under the same settings used for MPS and T3NS. Its runtime is also roughly twice as long as for the other two structures. In contrast, T3NS offers the most favorable trade-off between accuracy and computational cost: its mean error is about half that of MPS and significantly smaller than that of the leaf-only tree, while its runtime is only about 30%

longer than that of MPS.

TABLE I. Comparison of MPS, T3NS, and Leaf-only tree structures

Tree type	MPS	T3NS	Leaf-only
Number of lowest eigenstates (LOBPCG)	12	15	57
Mean error (LOBPCG)	0.385	0.354	0.317
Runtime in seconds (LOBPCG)	5.09×10^3	5.93×10^3	7.79×10^3
Number of lowest eigenstates (Inverse Iter.)	21	39	40
Mean error (Inverse Iter.)	0.067	0.033	22.214
Runtime in seconds (Inverse Iter.)	1.15×10^4	1.49×10^4	2.66×10^4

TABLE II: Eigenvalues and energy differences relative to ZPVE for acetonitrile.

Index	$E_{\text{ref}}/\text{cm}^{-1}$	LOBPCG (D=12)			II (D=20)		
		MPS	T3NS	Leaf-only	MPS	T3NS	Leaf-only
0	9837.407	0.026	0.024	0.019	0.001	0.000	0.000
1	360.990	0.011	0.011	0.011	0.001	0.001	0.001
2	360.990	0.011	0.012	0.011	0.001	0.001	0.001
3	723.179	0.028	0.028	0.024	0.002	0.002	0.003
4	723.179	0.029	0.029	0.026	0.002	0.002	0.003
5	723.825	0.083	0.092	0.048	0.007	0.005	0.003
6	900.659	0.024	0.008	0.023	0.005	0.002	0.000
7	1034.124	0.035	0.044	0.038	0.003	0.002	0.002
8	1034.124	0.055	0.049	0.040	0.006	0.002	0.002
9	1086.552	0.042	0.042	0.036	0.003	0.003	0.004
10	1086.552	0.042	0.045	0.040	0.003	0.003	0.004
11	1087.774	0.195	0.177	0.124	0.011	0.005	-0.000
12	1087.774	0.199	0.228	0.136	0.011	0.007	0.001
13	1259.809	0.006	-0.041	-0.002	0.013	0.004	0.002
14	1259.809	0.017	0.011	0.012	0.013	0.006	0.002
15	1388.967	0.493	0.291	0.289	0.061	0.032	0.167

TABLE II – continued from previous page

Index	$E_{\text{ref}}/\text{cm}^{-1}$	LOBPCG (D=12)			II (D=20)		
		MPS	T3NS	Leaf-only	MPS	T3NS	Leaf-only
16	1394.679	0.251	0.268	0.372	0.016	0.015	0.108
17	1394.679	0.270	0.274	0.445	0.020	0.018	0.094
18	1394.898	0.130	0.141	0.242	0.009	0.010	0.066
19	1397.680	0.414	0.288	0.363	0.070	0.037	0.095
20	1451.093	0.054	0.059	0.051	0.004	0.004	0.005
21	1451.093	0.055	0.059	0.051	0.004	0.004	0.005
22	1452.818	0.319	0.334	0.221	0.018	0.003	-0.001
23	1452.818	0.326	0.352	0.221	0.018	0.007	0.001
24	1453.394	0.369	0.390	0.240	0.016	0.009	-0.009
25	1483.219	-0.051	-0.036	-0.066	0.025	-0.003	-0.018
26	1483.220	-0.039	-0.023	-0.052	0.025	0.013	0.003
27	1620.199	0.011	-0.035	0.000	0.023	0.011	0.004
28	1620.199	0.022	-0.012	0.009	0.023	0.012	0.003
29	1620.744	0.408	0.309	0.276	0.042	0.027	0.002
30	1749.519	0.714	0.460	0.425	0.111	0.055	-0.663
31	1749.519	0.733	0.477	0.440	0.114	0.065	0.158
32	1756.412	0.502	0.525	0.622	0.031	0.037	-2.026
33	1756.412	0.524	0.555	0.659	0.036	0.046	-5.536
34	1757.119	0.426	0.431	0.541	0.036	0.035	-0.540
35	1757.119	0.463	0.451	0.555	0.041	0.037	0.096
36	1759.760	0.663	0.554	0.535	0.129	0.080	-2.494
37	1759.760	0.707	0.565	0.558	0.132	0.090	0.107
38	1785.177	-0.162	-0.117	-0.117	-0.041	-0.051	-0.055
39	1816.786	0.070	0.078	0.067	0.006	0.005	0.007
40	1816.786	0.072	0.079	0.069	0.006	0.005	0.007
41	1818.938	0.570	0.612	0.444	0.032	0.019	0.006
42	1818.939	0.572	0.613	0.445	0.032	0.019	0.005

TABLE II – continued from previous page

Index	$E_{\text{ref}}/\text{cm}^{-1}$	LOBPCG (D=12)			II (D=20)		
		MPS	T3NS	Leaf-only	MPS	T3NS	Leaf-only
43	1820.016	0.706	0.733	0.530	0.025	0.017	-0.002
44	1820.016	0.724	0.751	0.560	0.031	0.018	-0.003
45	1844.245	0.249	0.238	0.192	0.143	-0.595	-2.228
46	1844.316	0.326	0.402	0.250	0.086	0.090	-0.118
47	1844.317	0.366	0.483	0.293	0.094	0.094	-0.007
48	1844.676	0.355	0.537	0.221	0.097	0.088	-0.071
49	1931.514	0.049	0.009	-0.012	0.026	0.010	0.007
50	1931.514	0.097	0.027	0.003	0.066	0.012	0.009
51	1981.815	-0.080	-0.143	-0.057	0.034	0.019	0.006
52	1981.815	-0.068	-0.135	-0.053	0.035	0.020	0.006
53	1982.818	0.732	0.510	0.495	0.070	0.043	0.001
54	1982.818	0.736	0.584	0.522	0.070	0.045	0.000
55	2057.044	0.191	0.204	0.171	0.020	0.017	0.017
56	2065.265	0.145	0.131	0.108	0.011	0.012	0.009
57	2065.265	0.190	0.178	0.122	0.015	0.013	0.011
58	2111.364	0.934	0.675	0.630	0.196	0.119	0.116
59	2111.364	1.055	0.744	0.644	0.816	0.131	0.166
60	2112.281	1.362	1.042	0.778	0.214	0.155	0.162
61	2119.307	0.719	0.755	0.879	0.034	0.060	14.806
62	2119.307	0.748	0.795	0.922	0.057	0.077	0.248
63	2120.521	0.906	0.901	0.968	0.081	0.077	-0.996
64	2120.521	1.043	0.973	0.988	0.095	0.089	0.177
65	2120.889	0.912	0.966	0.888	0.079	0.075	-0.179
66	2122.816	1.024	0.813	0.785	0.196	0.133	-3.707
67	2122.816	1.070	0.962	0.819	0.205	0.148	0.054
68	2123.282	1.548	1.302	1.035	0.232	0.176	0.904
69	2142.444	-0.467	-0.329	-0.340	-0.029	-0.053	-0.062

TABLE II – continued from previous page

Index	$E_{\text{ref}}/\text{cm}^{-1}$	LOBPCG (D=12)			II (D=20)		
		MPS	T3NS	Leaf-only	MPS	T3NS	Leaf-only
70	2142.444	-0.435	-0.277	-0.335	-0.027	-0.048	-0.062
71	2183.617	0.090	0.096	0.088	0.008	0.006	0.009
72	2183.617	0.091	0.101	0.089	0.008	0.007	0.009
73	2186.117	0.929	0.959	0.785	0.040	0.020	0.009
74	2186.117	0.933	0.967	0.800	0.042	0.021	0.010
75	2187.618	1.243	1.262	0.954	0.047	0.032	-0.002
76	2187.618	1.259	1.287	0.971	0.060	0.034	0.002
77	2188.119	1.363	1.387	1.000	0.071	0.044	0.009
78	2206.608	0.038	0.131	0.176	0.168	0.206	-1450.636
79	2206.615	0.195	0.168	0.204	0.199	0.199	-109.094
80	2206.757	0.351	0.046	0.274	0.156	0.134	-107.196
81	2206.758	0.396	0.142	0.352	0.531	0.165	-1.451
82	2207.541	0.274	0.304	0.199	0.097	0.099	-14.246
83	2207.541	0.376	0.328	0.254	0.109	0.102	-182.294

IV. CONCLUSIONS

In this work, we developed and benchmarked a generalized tree tensor network framework for vibrational spectroscopy in which both the Hamiltonian and the wavefunction are represented as trees, i.e., a TTNO and a TTNS, respectively. Within this framework, we implemented and combined block LOBPCG and block inverse iteration methods. This approach achieves sub-wavenumber accuracy for two representative benchmark systems — a 64-dimensional bilinearly coupled oscillator model and acetonitrile as a real molecular system — demonstrating the capability to solve chemical physics problems with strong coupling and near-degeneracies.

In our comparison of tensor network topologies, MPS and T3NS yield similar wall-clock times, while leaf-only trees are significantly slower. At the same computational budget,

T3NS systematically delivers better accuracy than MPS for many states, consistent with its increased connectivity. The block formulations successfully address near-degeneracies, and the inverse-iteration refinement further reduces the errors obtained by LOBPCG alone.

All implementations used in this work are available as open-source code in the PyTreeNet ecosystem. The repository containing the TTNO/TTNS eigensolvers, input files for the oscillator and acetonitrile benchmarks, and scripts to reproduce the figures is publicly available at <https://github.com/sunshuo987/vibcal>. This enables full reproducibility and provides a platform for further developments, such as automated tree-structure optimization, improved preconditioners, and the computation of transition intensities for IR and Raman spectra.

ACKNOWLEDGMENTS

Shuo Sun acknowledges funding by the BMW Group.

The research is part of the Munich Quantum Valley, which is supported by the Bavarian state government with funds from the Hightech Agenda Bayern Plus.

We also like to thank the Munich Center for Quantum Science and Technology (MCQST) for support.

Appendix A: Scaling of the Compression Methods on Tree Tensor Networks

This appendix lists the tensor scaling of the TTNS-TTNO application methods mentioned in Sec. (II C 1). We consider D_O to be the maximum bond dimension in the TTNO, D_S the maximum bond dimension of the TTNS, χ the desired bond dimension of the MPS after the application, and d the maximum physical dimension. Note that κ is the maximum number of neighbours a node can have in a given tree. Thus $\kappa = 2$ for MPS and $\kappa = 3$ for T3NS. The scalings are listed in Table III.

TABLE III. The scaling for the different methods and different tree structures.

Tree	General	MPS	T3NS
Zip-Up	$\sum_{j=1}^{\kappa-1} dD_S^{\kappa-j+1} D_O^j \chi^j + d^2 D_S D_O^\kappa \chi^{\kappa-1}$ $+ d^2 D_S D_O \chi^{2\kappa-2}$	$dD_S^2 D_2 \chi + d^2 D_S D_O \chi^2$ $+ d^2 D_S D_O \chi^2$	$dD_S^3 D_O \chi + dD_S^2 D_O^2 \chi^2$ $+ d^2 D_S D_O \chi^4$
Direct			
Contraction	$d^2 D_S^\kappa D_O^\kappa + d^2 D_S D_O \chi^{2\kappa-2}$	$d^2 D_S^2 D_O^2 + d^2 \chi^2 D_1 D_2$	$d^2 D_S^3 D_O^3 + d^2 \chi^4 D_1 D_2$

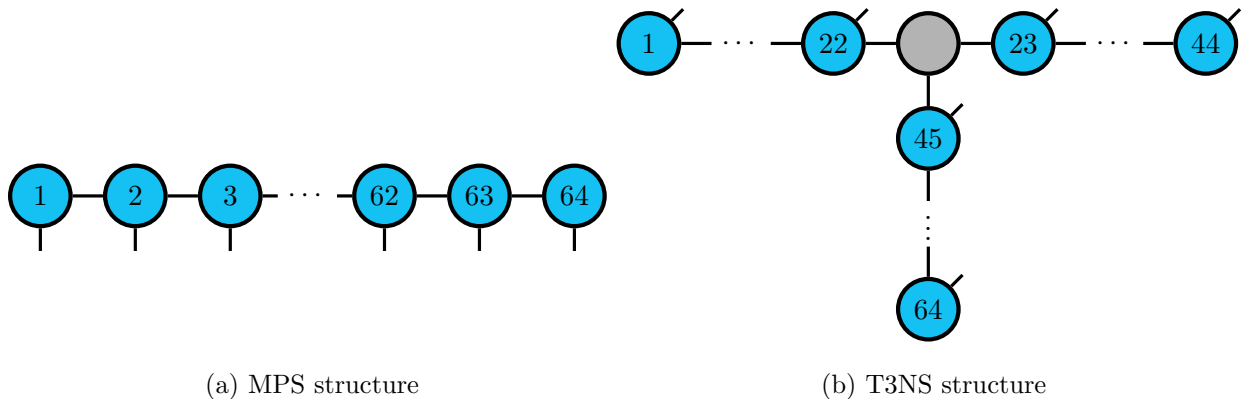
Appendix B: Tree structure used in the vibrational spectra calculations


FIG. 7. Tensor network structures used for the 64-dimensional coupled harmonic oscillator calculations. The blue circles denote nodes carrying physical legs, while the gray circles represent auxiliary tensor nodes.

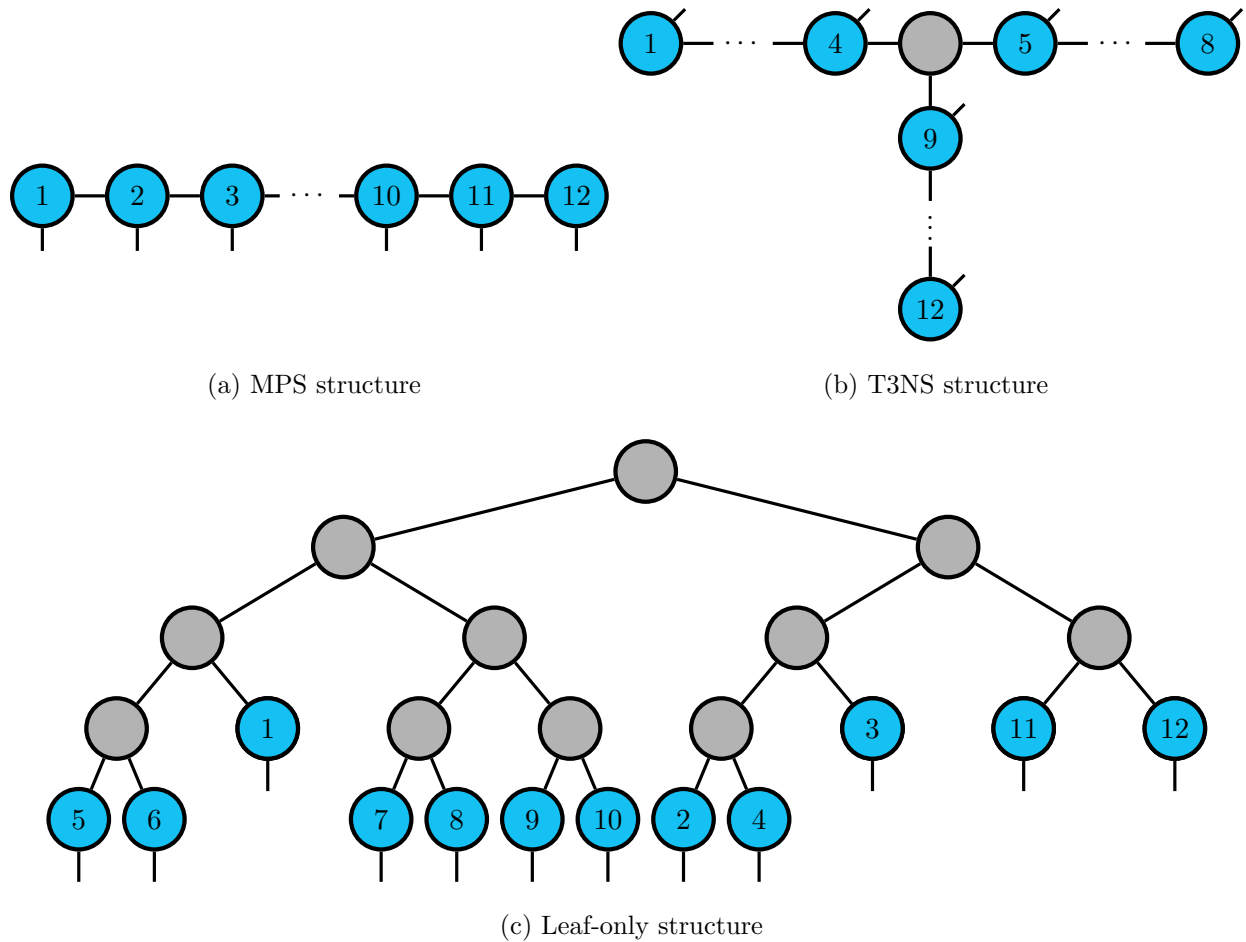


FIG. 8. Tensor network structures used for the acetonitrile (CH_3CN) vibrational spectra calculations. The blue circles denote nodes carrying physical legs, while the gray circles represent auxiliary tensor nodes.

REFERENCES

- ¹J. M. Bowman, “The self-consistent-field approach to polyatomic vibrations,” *Accounts of Chemical Research* **19**, 202–208 (1986).
- ²G. M. Chaban, J. O. Jung, and R. B. Gerber, “Ab initio calculation of anharmonic vibrational states of polyatomic systems: Electronic structure combined with vibrational self-consistent field,” *The Journal of Chemical Physics* **111**, 1823–1829 (1999).
- ³K. Yagi, T. Taketsugu, K. Hirao, and M. S. Gordon, “Direct vibrational self-consistent field method: Applications to H_2O and H_2CO ,” *The Journal of Chemical Physics* **113**, 1005–1017 (2000).

⁴T. K. Roy and R. B. Gerber, “Vibrational self-consistent field calculations for spectroscopy of biological molecules: New algorithmic developments and applications,” *Physical Chemistry Chemical Physics* **15**, 9468–9492 (2013).

⁵G. Rauhut, “Configuration selection as a route towards efficient vibrational configuration interaction calculations,” *The Journal of Chemical Physics* **127** (2007).

⁶D. Bégué, N. Gohaud, C. Pouchan, P. Cassam-Chenaï, and J. Liévin, “A comparison of two methods for selecting vibrational configuration interaction spaces on a heptatomic system: Ethylene oxide,” *The Journal of Chemical Physics* **127** (2007).

⁷M. Neff and G. Rauhut, “Toward large scale vibrational configuration interaction calculations,” *The Journal of Chemical Physics* **131** (2009).

⁸T. Mathea, T. Petrenko, and G. Rauhut, “Advances in vibrational configuration interaction theory-part 2: Fast screening of the correlation space,” *Journal of Computational Chemistry* **43**, 6–18 (2022).

⁹O. Christiansen, “Vibrational coupled cluster theory,” *The Journal of Chemical Physics* **120**, 2149–2159 (2004).

¹⁰P. Seidler and O. Christiansen, “Automatic derivation and evaluation of vibrational coupled cluster theory equations,” *The Journal of Chemical Physics* **131** (2009).

¹¹P. Seidler, M. Sparta, and O. Christiansen, “Vibrational coupled cluster response theory: A general implementation,” *The Journal of Chemical Physics* **134** (2011).

¹²B. Thomsen, K. Yagi, and O. Christiansen, “Optimized coordinates in vibrational coupled cluster calculations,” *The Journal of Chemical Physics* **140** (2014).

¹³Q. Zhang, R.-S. Wang, and L. Wang, “Neural canonical transformations for vibrational spectra of molecules,” *The Journal of Chemical Physics* **161** (2024).

¹⁴P. J. Ollitrault, A. Baiardi, M. Reiher, and I. Tavernelli, “Hardware efficient quantum algorithms for vibrational structure calculations,” *Chemical science* **11**, 6842–6855 (2020).

¹⁵S. Malpathak, S. D. Kallullathil, I. Loaiza, S. Fomichev, J. M. Arrazola, and A. F. Izmaylov, “Trotter simulation of vibrational Hamiltonians on a quantum computer,” *arXiv:2508.11865* (2025).

¹⁶M. Rakhuba and I. Oseledets, “Calculating vibrational spectra of molecules using tensor train decomposition,” *The Journal of Chemical Physics* **145** (2016).

¹⁷H. R. Larsson, “Computing vibrational eigenstates with tree tensor network states (TTNS),” *The Journal of Chemical Physics* **151** (2019).

¹⁸A. Baiardi, C. J. Stein, V. Barone, and M. Reiher, “Optimization of highly excited matrix product states with an application to vibrational spectroscopy,” *The Journal of Chemical Physics* **150** (2019).

¹⁹N. Glaser, A. Baiardi, and M. Reiher, “Flexible DMRG-based framework for anharmonic vibrational calculations,” *Journal of Chemical Theory and Computation* **19**, 9329–9343 (2023).

²⁰N. Glaser, A. Baiardi, A. Z. Lieberherr, and M. Reiher, “Vibrational entanglement through the lens of quantum information measures,” *The Journal of Physical Chemistry Letters* **15**, 6958–6965 (2024).

²¹H. R. Larsson and A. Viel, “2500 vibronic eigenstates of the NO₃ radical,” *Physical Chemistry Chemical Physics* **26**, 24506–24523 (2024).

²²H. R. Larsson, “A tensor network view of multilayer multiconfiguration time-dependent Hartree methods,” *Molecular Physics* **122**, e2306881 (2024).

²³H. R. Larsson, “Benchmarking vibrational spectra: 5000 accurate eigenstates of acetonitrile using tree tensor network states,” *The Journal of Physical Chemistry Letters* **16**, 3991–3997 (2025).

²⁴F. Fröwis, V. Nebendahl, and W. Dür, “Tensor operators: Constructions and applications for long-range interaction systems,” *Physical Review A* **81** (2010).

²⁵R. M. Milbradt, Q. Huang, and C. B. Mendl, “State diagrams to determine tree tensor network operators,” *SciPost Physics Core* **7** (2024).

²⁶Y.-Y. Shi, L.-M. Duan, and G. Vidal, “Classical simulation of quantum many-body systems with a tree tensor network,” *Physical Review A* **74** (2006).

²⁷K. Gunst, F. Verstraete, S. Wouters, O. Legeza, and D. Van Neck, “T3ns: Three-legged tree tensor network states,” *Journal of Chemical Theory and Computation* **14**, 2026–2033 (2018).

²⁸P. Carbonniere, D. Begue, A. Dargelos, and C. Pouchan, “Construction of an accurate quartic force field by using generalised least-squares fitting and experimental design,” *Chemical Physics* **300**, 41–51 (2004).

²⁹A. Leclerc and T. Carrington, “Calculating vibrational spectra with sum of product basis functions without storing full-dimensional vectors or matrices,” *The Journal of Chemical Physics* **140** (2014).

³⁰R. M. Milbradt, Q. Huang, and C. B. Mendl, “PyTreeNet: A python library for easy utilisation of tree tensor networks,” [arXiv:2407.13249](https://arxiv.org/abs/2407.13249) (2024).

³¹U. Schollwöck, “The density-matrix renormalization group in the age of matrix product states,” *Annals of Physics* **326**, 96–192 (2011).

³²G. Evenbly, “A practical guide to the numerical implementation of tensor networks I: Contractions, decompositions and gauge freedom,” [arXiv:2202.02138](https://arxiv.org/abs/2202.02138) (2022).

³³J. C. Bridgeman and C. T. Chubb, “Hand-waving and interpretive dance: An introductory course on tensor networks,” *J. Phys. A: Math. Theor.* **50** (2017).

³⁴P. Silvi, F. Tschirsich, M. Gerster, J. Jünemann, D. Jaschke, M. Rizzi, and S. Montangero, “The tensor networks anthology: Simulation techniques for many-body quantum lattice systems,” *SciPost Physics Lecture Notes* (2019).

³⁵R. Orús, “Tensor networks for complex quantum systems,” *Nature Reviews Physics* **1**, 538–550 (2019).

³⁶J. I. Cirac, D. Pérez-García, N. Schuch, and F. Verstraete, “Matrix product states and projected entangled pair states: Concepts, symmetries, theorems,” *Reviews of Modern Physics* **93** (2021).

³⁷M. C. Bañuls, “Tensor network algorithms: A route map,” *Annual Review of Condensed Matter Physics* **14**, 173–191 (2023).

³⁸H. Çakır, R. M. Milbradt, and C. B. Mendl, “Optimal symbolic construction of matrix product operators and tree tensor network operators,” *Physical Review B* **112** (2025).

³⁹W. Li, J. Ren, H. Yang, H. Wang, and Z. Shuai, “Optimal tree tensor network operators for tensor network simulations: Applications to open quantum systems,” *The Journal of Chemical Physics* **161** (2024).

⁴⁰A. V. Knyazev, “Toward the optimal preconditioned eigensolver: Locally optimal block preconditioned conjugate gradient method,” *SIAM journal on scientific computing* **23**, 517–541 (2001).

⁴¹A. Stathopoulos and K. Wu, “A block orthogonalization procedure with constant synchronization requirements,” *SIAM Journal on Scientific Computing* **23**, 2165–2182 (2002).

⁴²E. M. Stoudenmire and S. R. White, “Minimally entangled typical thermal state algorithms,” *New Journal of Physics* **12**, 055026 (2010).

⁴³P. Virtanen, R. Gommers, T. E. Oliphant, M. Haberland, T. Reddy, D. Cournapeau, E. Burovski, P. Peterson, W. Weckesser, J. Bright, S. J. van der Walt, M. Brett, J. Wilson,

K. J. Millman, N. Mayorov, A. R. J. Nelson, E. Jones, R. Kern, E. Larson, C. J. Carey, İ. Polat, Y. Feng, E. W. Moore, J. VanderPlas, D. Laxalde, J. Perktold, R. Cimrman, I. Henriksen, E. A. Quintero, C. R. Harris, A. M. Archibald, A. H. Ribeiro, F. Pedregosa, P. van Mulbregt, and SciPy 1.0 Contributors, “SciPy 1.0: Fundamental algorithms for scientific computing in Python,” [Nature Methods](#) **17**, 261–272 (2020).

⁴⁴D. Baye and P. H. Heenen, “Generalised meshes for quantum mechanical problems,” [Journal of Physics A: Mathematical and General](#) **19**, 2041–2059 (1986).

⁴⁵S. Dolgov, B. Khoromskij, I. Oseledets, and D. Savostyanov, “Computation of extreme eigenvalues in higher dimensions using block tensor train format,” [Computer Physics Communications](#) **185**, 1207–1216 (2014).

⁴⁶G. Avila and T. Carrington, “Using nonproduct quadrature grids to solve the vibrational schrödinger equation in 12d,” [The Journal of Chemical Physics](#) **134** (2011).